

# Search for a lighter Higgs Boson in Two Higgs Doublet Models

---

**Giacomo Cacciapaglia<sup>a</sup> , Aldo Deandrea<sup>a,1</sup> , Suzanne Gascon-Shotkin<sup>a</sup> , Solène Le Corre<sup>a,2</sup> , Morgan Lethuillier<sup>a</sup> , Junquan Tao<sup>b</sup>**

<sup>a</sup>*Univ. Lyon, Université Claude Bernard Lyon 1, CNRS/IN2P3, UMR5822 IPNL, F-69622, Villeurbanne, France*

<sup>b</sup>*Inst. High Energy Physics, Chinese Academy of Sciences, P.O. Box 918, Beijing 100049, China*

*E-mail:* [g.cacciapaglia@ipnl.in2p3.fr](mailto:g.cacciapaglia@ipnl.in2p3.fr), [deandrea@ipnl.in2p3.fr](mailto:deandrea@ipnl.in2p3.fr),  
[smgascon@in2p3.fr](mailto:smgascon@in2p3.fr), [s.le-corre@ipnl.in2p3.fr](mailto:s.le-corre@ipnl.in2p3.fr),  
[morgan.lethuillier@cern.ch](mailto:morgan.lethuillier@cern.ch), [taojq@ihep.ac.cn](mailto:taojq@ihep.ac.cn)

**ABSTRACT:** We consider present constraints on Two Higgs Doublet Models, both from the LHC at Run 1 and from other sources in order to explore the possibility of constraining a neutral scalar or pseudo-scalar particle lighter than the 125 GeV Higgs boson. Such a lighter particle is not yet completely excluded by present data. We show with a simplified analysis that some new constraints could be obtained at the LHC if such a search is performed by the experimental collaborations, which we therefore encourage to continue carrying out light diphoton resonance searches at  $\sqrt{s} = 13$  TeV in the context of Two Higgs Doublet Models.

**KEYWORDS:** Higgs bosons, Two Higgs doublet model, light scalar resonances, LHC

---

<sup>1</sup>also Institut Universitaire de France, 103 boulevard Saint-Michel, 75005 Paris, France

<sup>2</sup>leading author

---

## Contents

<b>1</b>	<b>Introduction</b>	<b>1</b>
<b>2</b>	<b>Two Higgs Doublet Models</b>	<b>2</b>
<b>3</b>	<b>Bounds on 2HDMs</b>	<b>3</b>
3.1	Indirect constraints	4
3.2	Direct LEP constraints	5
3.3	LHC Higgs boson constraints	5
<b>4</b>	<b>Search for a lighter scalar Higgs boson in the 2HDMs</b>	<b>6</b>
4.1	Cross sections and branching ratios	7
4.2	Constraining the 2HDMs parameter space	8
4.3	Comparison with the CMS low mass di-photon analysis	16
<b>5</b>	<b>Search for a light pseudo-scalar Higgs boson in the 2HDMs</b>	<b>19</b>
5.1	Computation of the cross-section value	19
5.2	Comparison with the CMS low mass di-photon analysis.	21
<b>6</b>	<b>Conclusions</b>	<b>23</b>

---

## 1 Introduction

After the discovery of a Higgs boson at the LHC in 2012 [1, 2], many studies, both from the theoretical and experimental side, have considered extensions of the Standard Model (SM) with an enlarged scalar sector. Concerning this scalar sector of physics beyond the Standard Model (BSM), most studies have considered the possibility of new scalars heavier than the 125 GeV Higgs boson which was discovered at the LHC. It is however possible to have a spectrum in which lighter scalars are present together with an SM-like Higgs boson at 125 GeV. Among these possibilities there are detailed BSM models as well as effective descriptions including only the extended scalar sector. Two Higgs Doublet Models (2HDMs) constitute one of the simplest possibilities, where the SM Lagrangian is extended by the addition of a second scalar doublet. Previous phenomenological studies describing the possibility of lighter Higgs bosons include [3–9], while for a recent study in supersymmetry (which naturally includes two doublets) we refer the reader to [10]. At masses below 125 GeV, the main search channel at the LHC is the di-photon decay channel [11, 12]. This paper is organised as follows: in Section 2 we describe the theoretical set-up adopted in our analysis; Section 3 is dedicated to the study of present constraints coming from flavour physics, electroweak precision tests,

theoretical bounds, direct LEP constraints on the scalar sector and LHC limits given by a 125 GeV Higgs boson; Section 4 contains the cross section and branch ratio calculations for a light scalar Higgs boson, a study of the parameter space of the different 2HDMs and a comparison with the CMS low mass di-photon analysis at 8 TeV [11]; Section 5 is dedicated to the study of the case where the lighter resonance is pseudo-scalar; finally we present our conclusions in Section 6 .

## 2 Two Higgs Doublet Models

We here briefly describe the theoretical framework of 2HDMs, see [13] for a general discussion. The 2HDMs are a simple extension of the Standard Model including two complex SU(2) doublets,  $\phi_1$  and  $\phi_2$ . In order to avoid flavour-changing neutral currents, one can introduce a  $\mathbb{Z}_2$  symmetry so that all fermions of a given electric charge couple to at most one Higgs doublet. These couplings can occur in different ways; the convention usually adopted is given in Table 1.

	Type I	Type II	Flipped (Type Y)	Lepton Specific (Type X)
Up-type quark	$\phi_2$	$\phi_2$	$\phi_2$	$\phi_2$
Down-type quark	$\phi_2$	$\phi_1$	$\phi_1$	$\phi_2$
Leptons	$\phi_2$	$\phi_1$	$\phi_2$	$\phi_1$

**Table 1:** The different possible couplings between the SM fermions and the two scalar doublets in 2HDMs.

The most generic 2HDMs potential constrained by the  $\mathbb{Z}_2$  symmetry can be written as:

$$V = m_{11}^2 \phi_1^\dagger \phi_1 + m_{22}^2 \phi_2^\dagger \phi_2 - m_{12}^2 \left( \phi_1^\dagger \phi_2 + \phi_2^\dagger \phi_1 \right) + \frac{\lambda_1}{2} \left( \phi_1^\dagger \phi_1 \right)^2 + \frac{\lambda_2}{2} \left( \phi_2^\dagger \phi_2 \right)^2 + \lambda_3 \left( \phi_1^\dagger \phi_1 \right) \left( \phi_2^\dagger \phi_2 \right) + \lambda_4 \left( \phi_1^\dagger \phi_2 \right) \left( \phi_2^\dagger \phi_1 \right) + \frac{\lambda_5}{2} \left[ \left( \phi_1^\dagger \phi_2 \right)^2 + \left( \phi_2^\dagger \phi_1 \right)^2 \right], \quad (2.1)$$

where all the parameters are real. The parameter  $m_{12}^2$  is responsible for a soft breaking of the  $\mathbb{Z}_2$  symmetry. The two scalar doublets acquire vacuum expectation values (vevs):

$$\phi_1 = \begin{pmatrix} 0 \\ \frac{v_1}{\sqrt{2}} \end{pmatrix}, \quad \phi_2 = \begin{pmatrix} 0 \\ \frac{v_2}{\sqrt{2}} \end{pmatrix}, \quad (2.2)$$

with  $v \equiv \sqrt{v_1^2 + v_2^2}$ .

After symmetry breaking we are left with five physical scalars: two neutral  $\mathcal{CP}$ -even states  $h$  and  $H$ , one neutral  $\mathcal{CP}$ -odd state  $A$  and two charged ones  $H^\pm$ . In order to move from the potential of eq. 2.1 to mass-eigenstates, one needs to introduce two angles:  $\beta$ , defined as

$\tan \beta = \frac{v_2}{v_1}$ , which rotates the two doublets in a basis where only one of them acquires a vev, and  $\alpha$  which mixes the  $\mathcal{CP}$ -even scalar states to give mass-eigenstates. The parameters of the potential can thus be translated into an equivalent set of parameters in the physical basis:

$$\begin{aligned} & \lambda_1, \lambda_2, \lambda_3, \lambda_4, \lambda_5, m_{11}^2, m_{22}^2, m_{12}^2 \\ & \Updownarrow \\ & m_h, m_H, m_A, m_{H^\pm}, \tan \beta, \sin(\beta - \alpha), v, m_{12}^2 \end{aligned} \tag{2.3}$$

where  $v$  is set to the electroweak scale, and one of the masses of the  $\mathcal{CP}$ -even states should be equal to the measured Higgs boson mass. The masses of the two  $\mathcal{CP}$ -even states are ordered with  $m_h < m_H$ , where we will call  $h$  the light Higgs boson and  $H$  the heavy Higgs boson of the model. The couplings between the neutral Higgs bosons and the fermions and gauge bosons are summarised in Table 2. In the rest of the study we will use the input parameters of the physical basis: we fix  $v = 246$  GeV and the heavy Higgs boson  $H$  of the model is identified with the Higgs boson discovered at LHC,  $m_H = 125$  GeV, while the remaining six parameters are left free.

		Type I	Type II	Flipped	Lepton Specific
Up-Type quark	h	$\frac{\cos \alpha}{\sin \beta}$			
	H	$\frac{\sin \alpha}{\sin \beta}$			
	A	$\cot \beta$			
Down-Type quark	h	$\frac{\cos \alpha}{\sin \beta}$	$-\frac{\sin \alpha}{\cos \beta}$	$-\frac{\sin \alpha}{\cos \beta}$	$\frac{\cos \alpha}{\sin \beta}$
	H	$\frac{\sin \alpha}{\sin \beta}$	$\frac{\cos \alpha}{\cos \beta}$	$\frac{\cos \alpha}{\cos \beta}$	$\frac{\sin \alpha}{\sin \beta}$
	A	$\cot \beta$	$\tan \beta$	$\tan \beta$	$\cot \beta$
Lepton	h	$\frac{\cos \alpha}{\sin \beta}$	$-\frac{\sin \alpha}{\cos \beta}$	$\frac{\cos \alpha}{\sin \beta}$	$-\frac{\sin \alpha}{\cos \beta}$
	H	$\frac{\sin \alpha}{\sin \beta}$	$\frac{\cos \alpha}{\cos \beta}$	$\frac{\sin \alpha}{\sin \beta}$	$\frac{\cos \alpha}{\cos \beta}$
	A	$\cot \beta$	$\tan \beta$	$\cot \beta$	$\tan \beta$
WW and ZZ	h	$\sin(\beta - \alpha)$			
	H	$\cos(\beta - \alpha)$			
	A	0			

**Table 2:** Tree level couplings between the neutral Higgs bosons and the gauge bosons and fermions normalised to their SM values for the different 2HDMs.

### 3 Bounds on 2HDMs

As we briefly discussed in the previous section, one of the simplest modifications of the SM consists in incorporating two scalar doublets, imposing custodial symmetry in order to allow satisfying the electroweak precision tests. The spectrum of neutral and charged scalars of the 2HDMs is a minimal extension of the scalar sector with one additional doublet and gives rise

to five physical scalars: two charged  $H^\pm$  and three neutral  $h$ ,  $H$  and  $A$  states. If the Higgs boson discovered at the LHC is associated with the heavier  $H$ , the two other neutral states can be a candidate for a lighter Higgs boson. The CMS collaboration has reported results on the search for a light resonance in di-photon final states [11], giving the observed upper limit at 95% confidence level (C.L.) on the cross section times branching ratio as a function of the mass of a light Higgs boson between 80 GeV and 110 GeV.

In the following we list the different constraints we use to impose bounds on the model. We split them in three classes: indirect constraints, LEP constraints and LHC constraints.

### 3.1 Indirect constraints

The indirect constraints we apply on the 2HDMs parameter space include limits on the oblique parameters S, T and U [14] due to electroweak precision tests, flavour constraints and theoretical requirements due to ensure stability of the potential, unitarity and perturbativity.

The oblique parameters are computed in the model via the program 2HDMC [15] and compared to the experimental limits [16] at  $2\sigma$  (see Table 3 for a recap of the updated experimental values with  $1\sigma$  uncertainties and the correlations between them).

	Experimental values		Correlations
S	$0.05 \pm 0.11$	ST	+0.90
T	$0.09 \pm 0.13$	SU	-0.59
U	$0.01 \pm 0.11$	TU	-0.83

**Table 3:** Experimental values of the oblique parameters with  $1\sigma$  uncertainty and correlations between them [16].

The stability of the potential is needed in order to allow symmetry breaking with a stable vacuum, thus the potential of the theory needs to be bounded from below. This condition requires [13]:

$$\begin{aligned} \lambda_1 &\geq 0, & \lambda_2 &\geq 0, & \lambda_3 &\geq -\sqrt{\lambda_1\lambda_2}, \\ \lambda_3 + \lambda_4 - |\lambda_5| &\geq -\sqrt{\lambda_1\lambda_2} \end{aligned} \quad (3.1)$$

In addition we require to have tree-level perturbative unitarity for the scattering of Higgs bosons and the longitudinal parts of electroweak gauge bosons [17].

In order to trust perturbative calculations, we add a condition on the quartic Higgs bosons couplings  $C_{h_i h_j h_k h_l}$ :

$$|C_{h_i h_j h_k h_l}| \leq 4\pi \quad (3.2)$$

The three conditions detailed above are also computed via the 2HDMC program.

Once the previous requirements are satisfied, the available parameter space is tested against flavour bounds. We look at the branching ratios  $\mathcal{BR}(\bar{B} \rightarrow X_s \gamma)$  and  $\mathcal{BR}(B_s \rightarrow$

$\mu^+\mu^-$ ), which obtain new contributions from the charged Higgs bosons and the neutral ones respectively and at the isospin asymmetry  $\Delta_0(B \rightarrow K^*\gamma)$  and the  $\Delta M_d$  frequency oscillation which are sensitive to the presence of charged Higgs bosons. The value of each process is computed in the 2HDMs via the program **SuperIso** [18, 19] and then compared to the experimental limits at  $2\sigma$ . In order to take into account the theoretical uncertainties in the 2HDMs calculation, which are not evaluated in **SuperIso**, we add to the experimental  $1\sigma$  uncertainty  $\sigma_{Exp}$  of each process the  $1\sigma$  theoretical uncertainty  $\sigma_{Th}$  of this same process computed in the SM given by the most recent theoretical calculations. The combined error  $\sigma_{comb}$  can then be obtained via:

$$\sigma_{comb} = \sqrt{\sigma_{Exp}^2 + \sigma_{Th}^2}$$

A summary of the results we use is available in Table 4.

Process	Experimental values	Theoretical computation	Combined error at $1\sigma$
$\mathcal{BR}(\bar{B} \rightarrow X_s \gamma)$	$(3.43 \pm 0.22) \times 10^{-4}$ [20]	$(3.40 \pm 0.19) \times 10^{-4}$ [21]	$0.29 \times 10^{-4}$
$\mathcal{BR}(B_s \rightarrow \mu^+ \mu^-)$	$(2.9 \pm 0.7) \times 10^{-9}$ [22, 23]	$(3.54 \pm 0.27) \times 10^{-9}$ [21]	$0.8 \times 10^{-9}$
$\Delta_0(B \rightarrow K^* \gamma)$	$(5.2 \pm 2.6) \times 10^{-2}$ [24]	$(5.1 \pm 1.5) \times 10^{-2}$ [21]	$3.0 \times 10^{-2}$
$\Delta M_d$	$0.510 \pm 0.003 \text{ ps}^{-1}$ [20]	$0.543 \pm 0.091 \text{ ps}^{-1}$ [25]	$0.091 \text{ ps}^{-1}$

**Table 4:** Values of the experimental and theoretical flavour constraints.

### 3.2 Direct LEP constraints

The **HiggsBounds** program [26–29] is a tool able to test a model against experimental data coming from LEP, Tevatron and the LHC. The program can be interfaced with **2HDMC** which will give appropriate inputs to **HiggsBounds**. In our analysis we use **HiggsBounds** version 4.2.1 with the LEP experiment constraints only, in order to impose LHC constraints separately. **2HDMC** gives **HiggsBounds** a parton-level input for the three scalar Higgs bosons and the two charged ones. The exclusion test at  $2\sigma$  is then performed on the five physical scalars of the theory. **HiggsBounds** returns a binary result indicating if the specific model point has been excluded at 95% C.L. or not.

### 3.3 LHC Higgs boson constraints

What we call “LHC constraints” are restrictions coming from experimental results on the 125 GeV Higgs boson, *i.e.* the 2HDM heavy Higgs boson  $H$ , in our case. To implement such limits, we use the exclusion contours in the plane of the signal strength for each individual production mode  $\mu_{VBF/VH}$  vs  $\mu_{ggh/tth}$  given by the combined ATLAS and CMS experiments at Run 1 [30]. Assuming a Gaussian profile for the likelihood  $\mathcal{L}$  at 68% C.L., each exclusion

contour for a specific decay channel  $Y$  obeys the following equation:

$$\begin{aligned} -2\log \mathcal{L}_Y &\equiv \chi_Y^2 \\ &= \begin{pmatrix} \mu_{ggH/ttH} - \hat{\mu}_{ggH/ttH,Y} \\ \mu_{VBF/VH} - \hat{\mu}_{VBF/VH,Y} \end{pmatrix}^T \begin{pmatrix} a_Y & b_Y \\ b_Y & c_Y \end{pmatrix} \begin{pmatrix} \mu_{ggH/ttH} - \hat{\mu}_{ggH/ttH,Y} \\ \mu_{VBF/VH} - \hat{\mu}_{VBF/VH,Y} \end{pmatrix}, \end{aligned} \quad (3.3)$$

where  $\hat{\mu}_{ggH/ttH,Y}$  and  $\hat{\mu}_{VBF/VH,Y}$  are the data best fit values and  $a_Y$ ,  $b_Y$  and  $c_Y$  are the parameters of the ellipse. These five parameters fully describe the ellipse. We fit the ellipses for each decay channel  $Y = \{WW, ZZ, \gamma\gamma, \tau\tau, b\bar{b}\}$  and hence obtained the parametrisation for each of them (see [31] for more details). We then compute the  $\chi_Y^2$  value in the 2HDM using equation 3.3. For this, we assume the following relations:

$$\begin{cases} \mu_{ggH/ttH,Y} = \frac{(\sigma_{gg \rightarrow H}^{2HDM} + \sigma_{tt \rightarrow H}^{2HDM}) \times BR_Y^{2HDM}}{(\sigma_{gg \rightarrow H}^{SM} + \sigma_{tt \rightarrow H}^{SM}) \times BR_Y^{SM}} \simeq \kappa_g^2 \times \frac{BR_Y^{2HDM}}{BR_Y^{SM}} \\ \mu_{VBF/VH,Y} = \frac{(\sigma_{VBF}^{2HDM} + \sigma_{VH}^{2HDM}) \times BR_Y^{2HDM}}{(\sigma_{VBF}^{SM} + \sigma_{VH}^{SM}) \times BR_Y^{SM}} \simeq \kappa_V^2 \times \frac{BR_Y^{2HDM}}{BR_Y^{SM}} \end{cases} \quad (3.4)$$

with  $\kappa_g^2 \equiv \frac{\Gamma_{H \rightarrow gg}^{2HDM}}{\Gamma_{H \rightarrow gg}^{SM}}$ ,  $\kappa_V^2 \equiv \frac{\Gamma_{H \rightarrow WW}^{2HDM}}{\Gamma_{H \rightarrow WW}^{SM}} = \cos^2(\beta - \alpha)$  (see Table 2).

Combining the log-likelihood ratios, we obtain:

$$\Delta\chi^2(p_j) = \sum_Y \chi_Y^2(p_j) - \sum_Y \chi_Y^2(\hat{p}_j), \quad (3.5)$$

with  $p_j$  the set of free parameters on which the function depends and  $\hat{p}_j$  their value minimising the  $\chi^2$  function. According to Wilks's theorem, the  $\Delta\chi^2$  function follows a  $\chi^2$  distribution with a number of degrees of freedom equal to the number of free parameters. In our case, we have six degrees of freedom ( $\kappa_g^2$ ,  $\kappa_V^2$ ,  $BR_{H \rightarrow WW}^{2HDM}$ ,  $BR_{H \rightarrow \tau\tau}^{2HDM}$ ,  $BR_{H \rightarrow \gamma\gamma}^{2HDM}$ ,  $BR_{H \rightarrow b\bar{b}}^{2HDM}$ , as  $BR_{H \rightarrow ZZ}^{2HDM}$  is linked to  $BR_{H \rightarrow WW}^{2HDM}$ ). This choice in the free parameters implies that we assume there is no correlation between the kappas and the branching ratios, which is correct as long as the deviation of the branching ratio is not too large with respect to the Standard Model values. A point in the 2HDM parameter space passing the LHC constraints, therefore, has a  $\Delta\chi^2$  value lower than 12.85, which is the value at 95% C.L. for a 6 degrees-of-freedom  $\chi^2$  distribution.

#### 4 Search for a lighter scalar Higgs boson in the 2HDMs

A light resonance decaying into two photons is being searched for by CMS [11] in the range of mass between 80 and 110 GeV. In this section we will explore the possibility that the signal may be given by the light scalar state in the 2HDMs. To compare with the experimental sensitivity (in particular at 8 TeV), we need to compute the expected production cross sections in the different production modes and branching ratios into the observed final states. In the following subsections we illustrate the procedure we followed and the results used in the present work to obtain restrictions on the parameter space of the various 2HDMs. In 4.1

we discuss the calculation method used for cross sections times branching ratios. Then we apply, in section 4.2, the present bounds coming from the three sets of constraints defined in the previous section in order to define the available parameter space. We finally test the sensitivity of the CMS low mass di-photon analysis at the LHC Run 1, in section 4.3, in the available parameter space for the four types of 2HDMs. To do so, we rely on a scan on the six free parameters in the physical basis.

#### 4.1 Cross sections and branching ratios

We use the program 2HDMC [15] version 1.7.0 to compute the branching ratios of the different Higgs bosons of the theory. As input, the program requires a numerical value for each of the seven parameters of the physical basis and provides, as output, the total width, branching ratios and couplings at next to leading order (NLO) for each Higgs boson.

The cross sections can also be computed via programs like **SusHi** [32]: however, the output is restricted to the gluon fusion and  $b\bar{b}$  production modes while **SusHi** does not provide vector boson fusion production (VBF) nor associated production with gauge bosons (VH). In order to overcome this restriction, and to quicken the calculation, we compute the cross sections using an approximation that we have briefly introduced in section 3.3 and that we denote in the following as the “kappa trick”. Defining the generic parameter  $\kappa_Y$  as  $\kappa_Y^2 = \frac{\Gamma_Y^{2HDM}}{\Gamma_Y^{SM}}$  for a specific decay channel  $Y$ , we approximate the cross sections as:

$$\sigma_{ggh}^{2HDM} \simeq \kappa_g^2 \times \sigma_{ggh}^{SM}, \quad \sigma_{VBF/VH}^{2HDM} \simeq \kappa_V^2 \times \sigma_{VBF/VH}^{SM} = \sin^2(\beta - \alpha) \times \sigma_{VBF/VH}^{SM}. \quad (4.1)$$

The second equation has such a simple form because, as the couplings of the light scalar Higgs boson to the W and Z bosons are rescaled in the same way compared to the SM couplings (cf Table 2), then  $\kappa_Z = \kappa_W \equiv \kappa_V = \sin(\beta - \alpha)$ . The SM cross section is taken from the LHC Higgs Cross-Section Working Group [33]. The kappas are computed thanks to the output given by 2HDMC. Hence we are able to compute the cross section times branching ratio of the two neutral scalar Higgs bosons using only the 2HDMC program, via equation 4.1.

It is pertinent at this point to comment on the level of validity of this approximation. The cross section production in VBF and VH mode should not cause any problem as the leading effect arises at tree level, however for the gluon fusion mode a loop induced coupling is present and thus it is important to check the validity of the “kappa trick” for this production mode. Note indeed that for loop induced vertices the use of an effective kappa factor is not always appropriate and more general parameterisations exist (see for example [34, 35]). In order to explore this issue and establish if this simple approximation could be used, we perform a comparison between the cross sections in gluon fusion obtained via the program **SusHi** and the ones obtained with the “kappa trick”. As 2HDMC only considers NLO corrections, we also ran **SusHi** at NLO. The SM inputs required by the two programs are set to the recommended values given by the Particle Data Group [24] summarised in Table 5. The 2HDM inputs used are given in Table 6: we chose to fix all the parameters except the mass of the light neutral scalars, whose cross section we want to test. We use **SusHi** version 1.6.0 together with **LHAPDF**



6.1.6 [36]. The parton distribution functions used in the program are `MMHT201468c1` for LO and `PDF4LHC15_mc` for NLO and NNLO [37]. The renormalization and factorization scales  $\mu_R$  and  $\mu_F$  for the gluon fusion process are set to  $\mu_R = \mu_F = m_\phi/2$  with  $\phi = \{h, H, A\}$  [38]. The  $b\bar{b}$  production mode proposed by `SusHi` is turned off.

$m_W$ (GeV)	$\Gamma_W$ (GeV)	$m_Z$ (GeV)	$\Gamma_Z$ (GeV)	$\bar{m}_b(m_b)$ (GeV)	$m_t(\text{pole})$ (GeV)
80.385	2.085	91.1876	2.4952	4.18	173.34

$m_c(\text{pole})$ (GeV)	$\alpha_{EM}$	$\alpha$	$\alpha_s$	$G_F$ (GeV) $^{-2}$
1.76	1/127.934	1/137.0359991	0.118	$1.16637 \times 10^{-5}$

**Table 5:** SM input parameters [24].

Fixing six of the seven free parameters, we allow only  $m_h$  to vary between 80 to 110 GeV with a step of 1 GeV between each point (see Table 6). The results are plotted in Figure 1. The dashed blue line corresponds to the cross section computed with the “kappa trick”, the dotted red line to the computation with `SusHi` and the solid green line to the deviation between the two, computed as:

$$\Delta \equiv \frac{\sigma_{gg \rightarrow h}^{\text{kappa trick}} - \sigma_{gg \rightarrow h}^{\text{SusHi}}}{\sigma_{gg \rightarrow h}^{\text{SusHi}}} \times 100. \quad (4.2)$$

$m_h$ (GeV)	$m_H$ (GeV)	$m_A$ (GeV)	$m_{H^\pm}$ (GeV)	$\tan \beta$	$\sin(\beta - \alpha)$	$m_{12}$ (GeV)
[80;110], step 1.	125	550	600	5	-0.2	30

**Table 6:** Input parameters in the 2HDM Type I for the comparison between `SusHi` and “kappa trick” cross sections.

The plot shows a deviation of less than 3% for the whole mass range and this deviation is stable upon modification of the values of the input parameters (see Figure 16 in the appendix). As it stays within the range allowed by the uncertainties (theoretical, PDF and  $\alpha_s$ ) calculated by the LHC Higgs Cross-Section Working Group [33], we consider this test as having validated our method for the light Higgs boson. For completeness, we make a similar analysis for the heavy Higgs boson at 125 GeV (see Figure 17 in the appendix) finding deviations less than 1% at  $m_H = 125$  GeV. In the rest of the study, therefore, we will use the “kappa trick” approximation to compute the cross section of the light and heavy scalar Higgs bosons in the 2HDMs.

## 4.2 Constraining the 2HDMs parameter space

In this section we study the influence of the three sets of constraints defined in Section 3 (indirect, LEP and LHC constraints) on the free parameters. For this purpose we generate

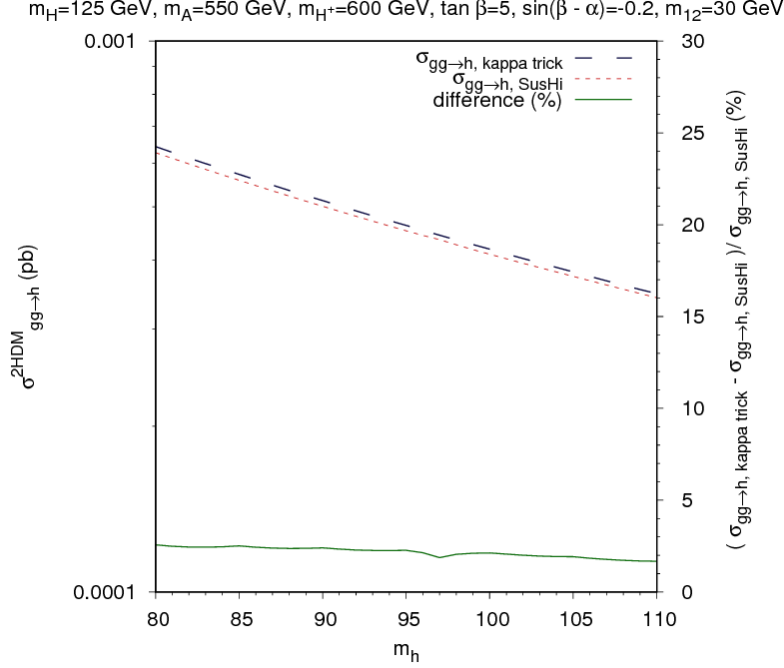


**Figure 1:**  $\sigma_{gg \rightarrow h}^{2HDM}$  computed with the “kappa trick” (dashed blue line), with SusHi (dotted red line) and the deviation between the two (solid green line).

a set of one million points for each of the four different types of model defined in Table 1 with random values for each of the free parameters. The available ranges we use in the simulation are given in Table 7. The range of variation for  $m_h$  corresponds to the mass range available in the CMS di-photon analysis. The lower bound of 80 GeV for  $m_{H^\pm}$  comes from the bound obtained at the LEP experiment [39]. The ranges for  $m_A$  and  $m_{12}^2$ , although not totally general, are the result of previous quick scans that we will not show in this paper and which eliminate areas with a very low density of points passing the three sets of constraints (indirect, LEP and LHC constraints).

Once the points are generated, we impose the three kinds of constraints detailed above: indirect ones, direct LEP and LHC Higgs boson ones.

$m_h$ (GeV)	$m_H$ (GeV)	$m_A$ (GeV)	$m_{H^\pm}$ (GeV)	$\sin(\beta - \alpha)$	$\tan \beta$	$m_{12}^2$ (GeV) <sup>2</sup>
[80;110]	125	[60;1000]	[80;1000]	[-1;1]	[1/50;50]	[-(300) <sup>2</sup> ;+(200) <sup>2</sup> ]

**Table 7:** Range of variation for the free parameters used in the analysis.

In Figure 2, all the generated points are plotted in the plane  $m_A$  vs  $m_{H^\pm}$ . The upper left panel corresponds to Type I, the upper right to Type II, the lower left to the Flipped model and the lower right to Lepton Specific model. The points passing only the indirect constraints

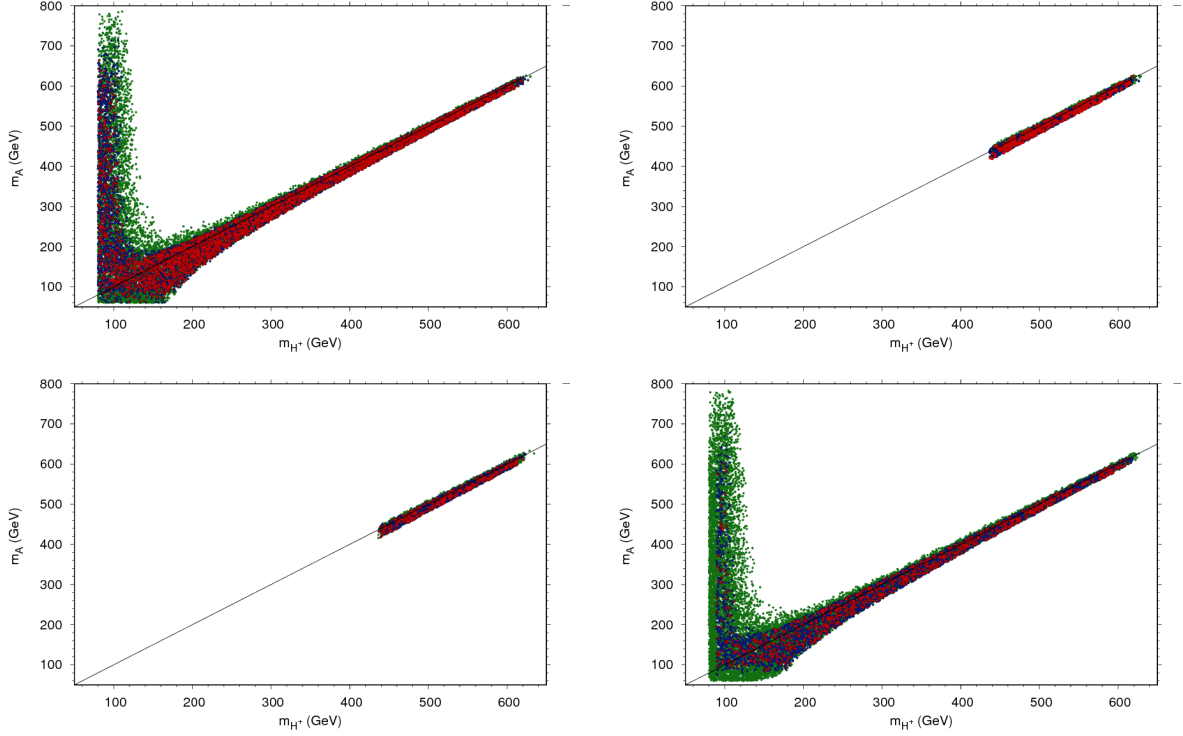


**Figure 2:** Constraints on the free parameters in the plane  $m_A$  vs  $m_{H^\pm}$ . Top left: Type I. Top right: Type II. Bottom left: Flipped. Bottom right: Lepton Specific. In green: points passing indirect constraints only. In blue: points passing indirect and LEP constraints. In red: points passing indirect, LEP and LHC constraints.

are plotted in green, those passing indirect and LEP constraints are in blue and those passing indirect, LEP and LHC constraints are in red. We will use these same conventions in the rest of this section.

Firstly we can see that the  $m_A$  and  $m_{H^\pm}$  masses are very correlated: when  $m_A$  and  $m_{H^\pm}$  grow, the indirect constraints force them to be near the black line corresponding to  $m_A = m_{H^\pm}$ . This is due to the T parameter which is very sensitive to these two masses and enforces them to be close to each other. Looking only at the red points, those which pass the three sets of constraints we defined previously, we can see that the two masses are bounded. In Type I, we find that most of the red points lie in the ranges  $m_A \in [60 \text{ GeV}; 650 \text{ GeV}]$  and  $m_{H^\pm} \in [80 \text{ GeV}; 630 \text{ GeV}]$ . In Type II and Flipped, the two masses are much more constrained  $m_A \in [400 \text{ GeV}; 650 \text{ GeV}]$  and  $m_{H^\pm} \in [430 \text{ GeV}; 630 \text{ GeV}]$ : this is due to the fact that the down-type quarks couple now to the  $\phi_1$  doublet instead of the  $\phi_2$  doublet as in Type I, thus the  $\mathcal{BR}(B \rightarrow X_s \gamma)$  flavour limit imposes a very strong constraint on the mass of the charged Higgs bosons (see Figure 18 in the appendix). Associated with the T parameter constraint, it imposes also the bounds on the pseudo-scalar mass. The Lepton Specific case is very similar to Type I as the couplings of the down-type quark are the same.

We find  $m_A \in [80 \text{ GeV}; 630 \text{ GeV}]$  and  $m_{H^\pm} \in [80 \text{ GeV}; 630 \text{ GeV}]$  to be the preferred regions. We should remark that these bounds are not absolute and that there may be red points exceeding these bounds. However, our simulation shows that the bulk of the allowed points are inside the ranges, so that we decided to use them in order to increase the statistics of our scan.

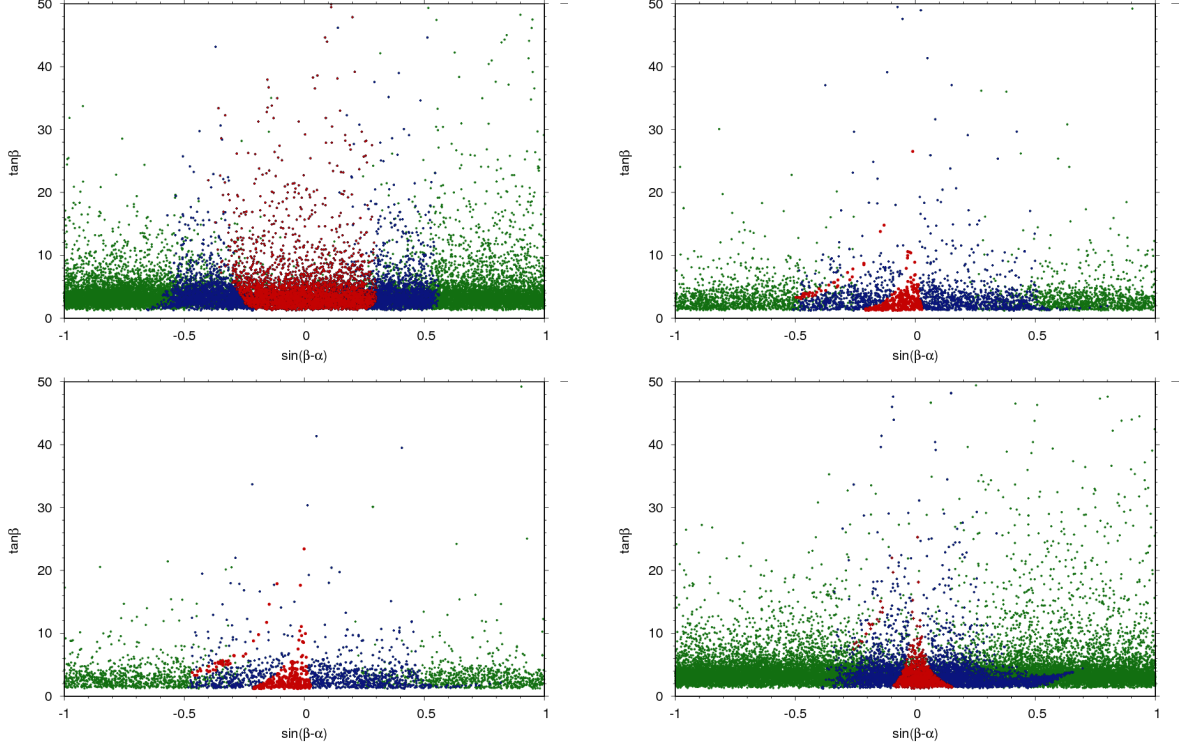


**Figure 3:** Constraints on the free parameters in the plane  $\tan \beta$  vs  $\sin(\beta - \alpha)$ . Top left: Type I. Top right: Type II. Bottom left: Flipped. Bottom right: Lepton Specific. Same colour code as in Figure 2.

Looking now at the plane  $\tan \beta$  vs  $\sin(\beta - \alpha)$  (shown in Figure 3) we can constrain in the same way the  $\tan \beta$  parameter. If it is difficult to impose an upper limit in all types as we lack statistics for high values of  $\tan \beta$  and we see a few red points up to the upper value, nevertheless we can impose a lower bound of  $\tan \beta > 1.2$  for the four different types.

The bounds on  $\sin(\beta - \alpha)$  can be more easily seen in the plane  $m_h$  vs  $\sin(\beta - \alpha)$  (shown in Figure 4): we see that  $m_h$  is not constrained as red points span the whole range of masses. For  $\sin(\beta - \alpha)$ , the allowed range is close to zero, which is consistent with our choice of  $m_H = 125 \text{ GeV}$ : as  $\sin(\beta - \alpha) \simeq 0$ , we have  $\cos(\beta - \alpha) \simeq 1$  which means that the couplings of the heavy Higgs boson  $H$  to the gauge bosons are close to the SM ones. We are therefore close to the alignment limit [8]. We find that the preferred ranges are  $\sin(\beta - \alpha) \in [-0.4; 0.3]$  for Type I,  $\sin(\beta - \alpha) \in [-0.5; 0.05]$  for Type II and Flipped model and  $\sin(\beta - \alpha) \in [-0.3; 0.2]$  for Lepton Specific model.

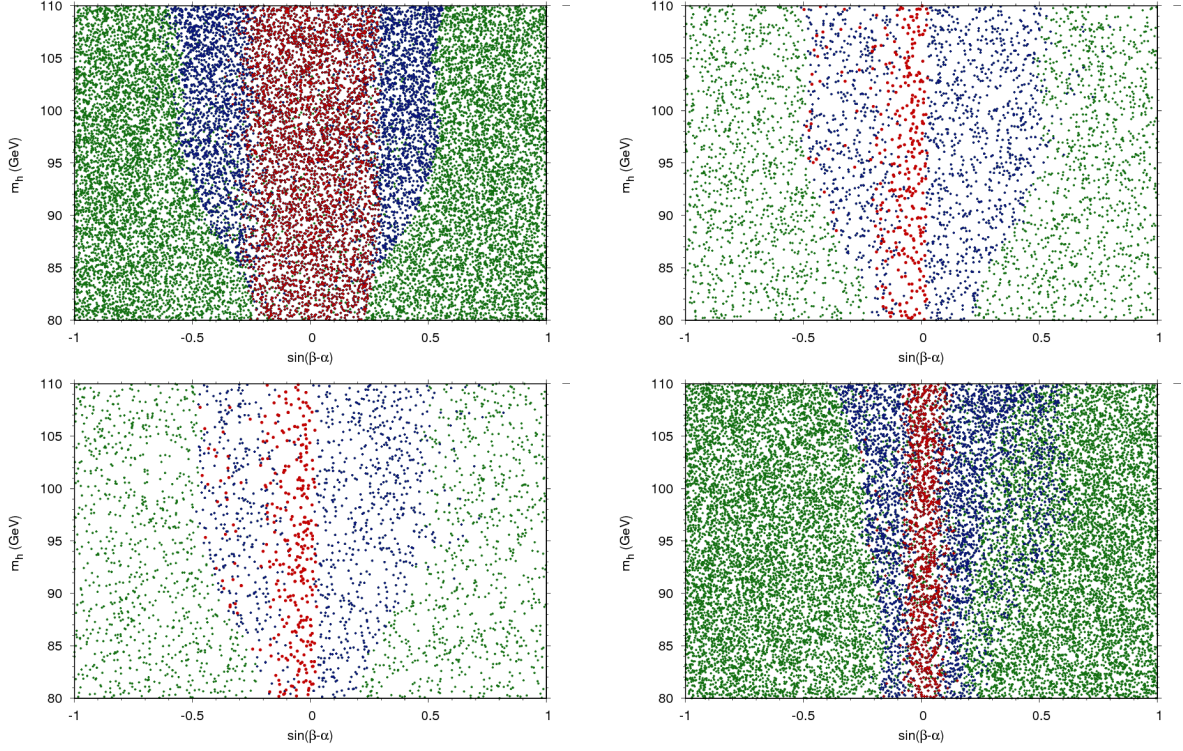


**Figure 4:** Constraints on the free parameters in the plane  $m_h$  vs  $\sin(\beta - \alpha)$ . Top left: Type I. Top right: Type II. Bottom left: Flipped. Bottom right: Lepton Specific. Same colour code as in Figure 2.

Finally, looking at the plane  $m_{12}$  vs  $\sin(\beta - \alpha)$  we can constrain the last free parameter (see Figure 5). We cannot put any lower bound on  $m_{12}^2$  but we find  $m_{12}^2 < (100 \text{ GeV})^2$  in the four different types.

The previous results show that the range of the free parameters can be further limited in order to increase the statistics of the allowed points. In addition to this, as we are interested in checking the sensitivity to a lighter Higgs boson at LHC Run 1 in the di-photon decay channel, we can further restrict the areas of interest to where the red points correspond to relatively high values of cross section times branching ratio to two photons. The minimum value of the CMS observed upper limit [11] is 0.032 pb in the gluon fusion channel, obtained for  $m_h = 103 \text{ GeV}$  and 0.019 pb in the VBF/VH channel, obtained for  $m_h = 100.5 \text{ GeV}$ . Keeping these values in mind, we can look at the predicted 2HDM cross-section times branching ratio values as a function of  $\sin(\beta - \alpha)$ . We plot the results for the gluon fusion production mode in Figure 6 and for VBF/VH production mode in Figure 7. The red dotted line corresponds to the minimum value of the CMS observed upper limit for each of the production modes. If all the red points are below this line, it means that CMS was not sensitive to a lighter Higgs boson in this particular channel at LHC Run 1.

The first important result we can extract from these figures is that in the Type II, Flipped



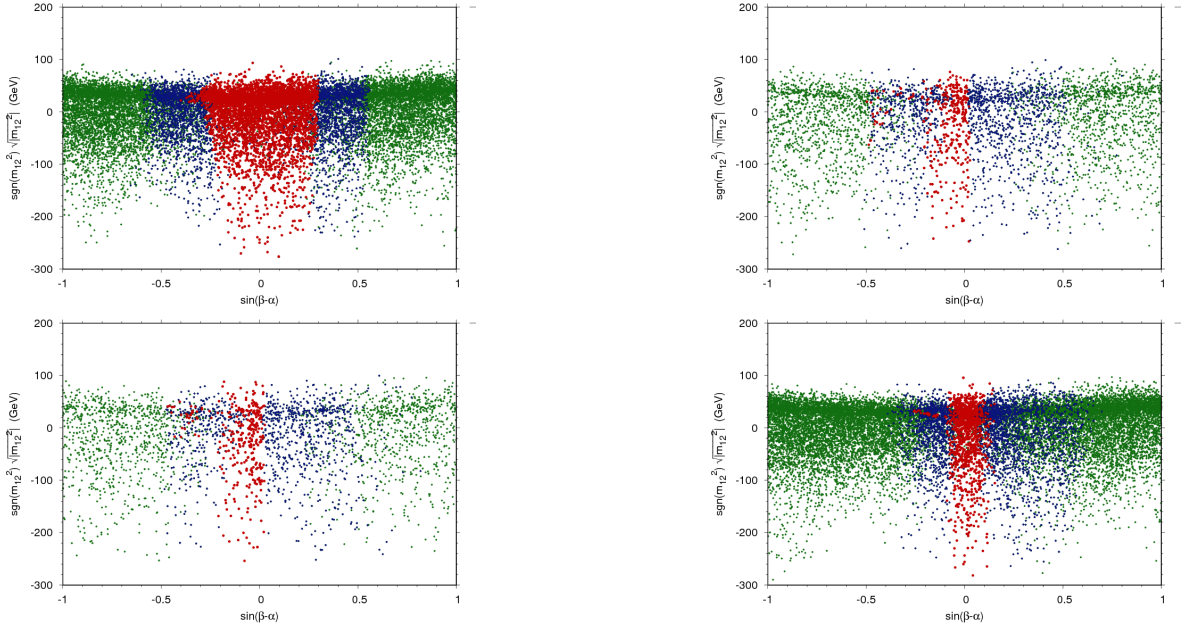


**Figure 5:** Constraints on the free parameters in the plane  $m_{12}$  vs  $\sin(\beta - \alpha)$ . Top left: Type I. Top right: Type II. Bottom left: Flipped. Bottom right: Lepton Specific. Same colour code as in Figure 2.

and Lepton Specific models, CMS had no sensitivity to a lighter Higgs boson at LHC Run 1 in the  $h \rightarrow \gamma\gamma$  decay channel, neither in the gluon fusion nor in the VBF/VH production mode. Therefore we will not carry on with these types any further. Looking at the results for Type I, we can see that there is no sensitivity in the gluon fusion channel. However, in the VBF/VH channel, we find red points above the dashed line. As the value of the CMS observed upper limit depends on the mass of the light Higgs boson considered, the dashed line represented on the plots is not an absolute bound. Some of the red points above it can be *de facto* below the CMS observed limit, but it is a good indication of the potential capability of the channel for some exclusion. We can therefore expect to have some sensitivity in the VBF/VH channel.

We can exploit Figure 7 even further by choosing to look only at areas where the points have relatively high values of cross section times branching ratio, i.e. areas where the points are close to the CMS analysis limit sensitivity. We choose a lower bound at 0.01 pb to select the points, which corresponds to  $\sin(\beta - \alpha) \in [-0.3; -0.05]$ .

We can similarly work with tighter ranges for the parameters  $\tan \beta$  and  $m_{12}^2$  (see Figure 8). We choose  $\tan \beta \in [2; 12]$  and  $m_{12}^2 \in [-(100 \text{ GeV})^2; +(100 \text{ GeV})^2]$ .

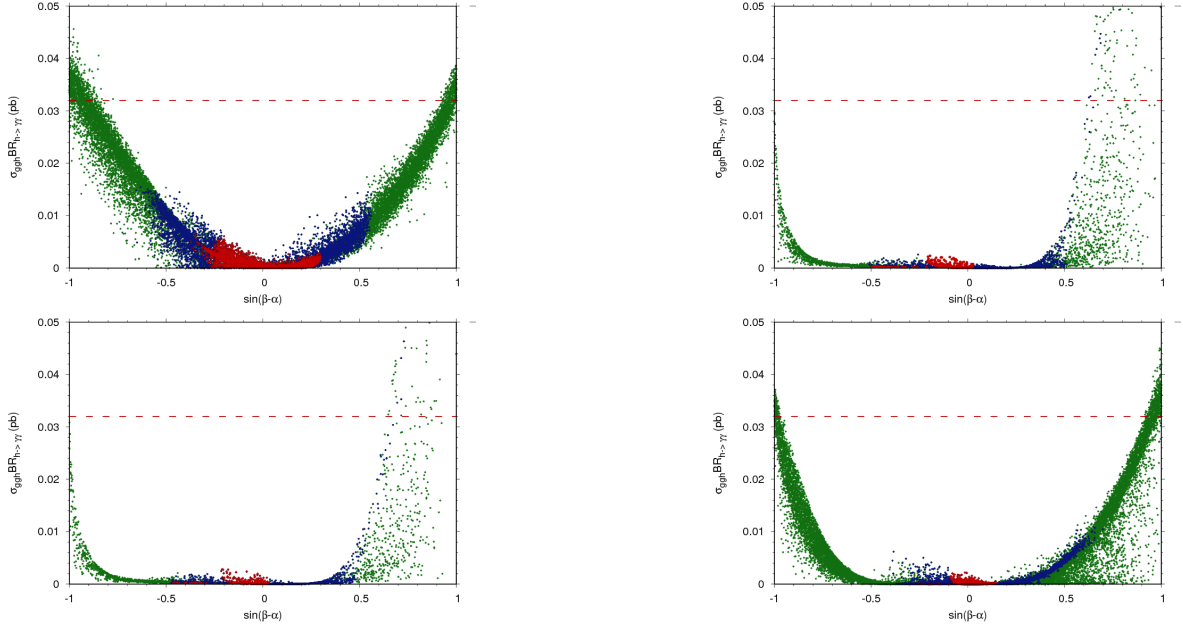


**Figure 6:** 2HDM generated points in the plane  $\sigma \times BR_{h \rightarrow \gamma\gamma}$  vs  $\sin(\beta - \alpha)$  in the gluon fusion production mode. Top left: Type I. Top right: Type II. Bottom left: Flipped. Bottom right: Lepton Specific. Same colour code as in Figure 2. The dashed line corresponds to the minimum value of the CMS observed upper limit in the gluon fusion production mode.

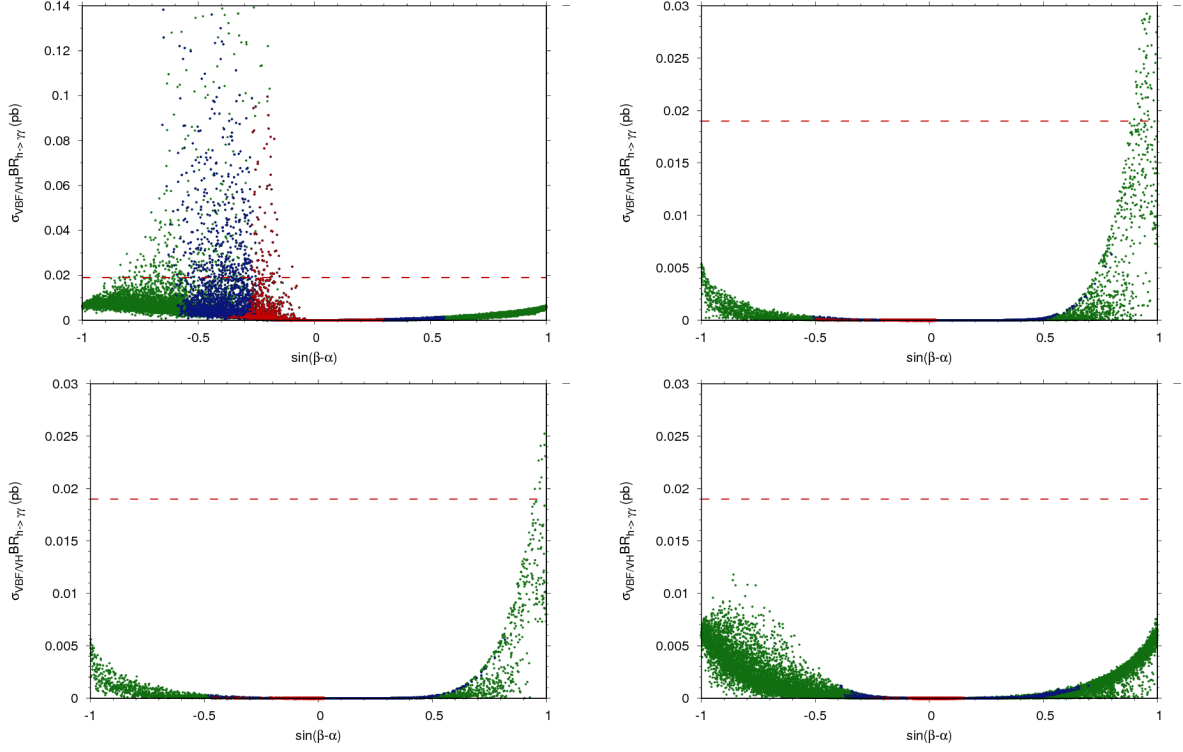


**Figure 7:** 2HDM generated points in the plane  $\sigma \times BR_{h \rightarrow \gamma\gamma}$  vs  $\sin(\beta - \alpha)$  in the VBF/VH production mode. Top left: Type I. Top right: Type II. Bottom left: Flipped. Bottom right: Lepton Specific. Same colour code as in Figure 2. The dashed line corresponds to the minimum value of the CMS observed upper limit in the VBF/VH production mode.

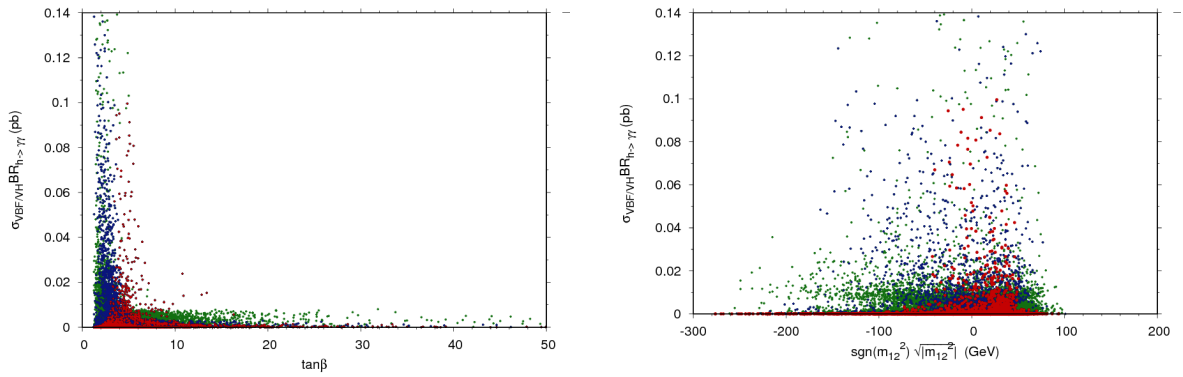


**Figure 8:** Value of the cross section times branching ratio in the VBF/VH production mode as a function of  $\tan\beta$  (left) and  $\text{sgn}(m_{12}) \times \sqrt{|m_{12}^2|}$  (right) in Type I. Same colour code as in Figure 2.



After having defined the allowed parameter region, and the more promising region with respect to the di-photon search, we are now ready to perform a second “focused” simulation and make a detailed comparison with the sensitivity of the CMS search at 8 TeV.

### 4.3 Comparison with the CMS low mass di-photon analysis

We thus perform a new scan with one million points, this time for Type I only, using the restricted parameter ranges we found in the previous section (see Table 8). We remind the reader that for  $m_A$  and  $m_{H^\pm}$  the new range results only from the three sets of constraints (the indirect, LEP and LHC constraints) we imposed. For the parameters  $\sin(\beta - \alpha)$ ,  $\tan \beta$  and  $m_{12}^2$  it results from our choice to restrict the scan to areas with large value of  $\sigma_{VBF/VH} \times BR_{h \rightarrow \gamma\gamma}$  (above 0.01 pb), as explained in Section 4.2.

$m_h$ (GeV)	$m_H$ (GeV)	$m_A$ (GeV)	$m_{H^\pm}$ (GeV)	$\sin(\beta - \alpha)$	$\tan \beta$	$m_{12}^2$
[80;110]	125	[60;650]	[80;630]	[-0.3;-0.05]	[2;12]	[-(100) <sup>2</sup> ;+(100) <sup>2</sup> ]

**Table 8:** Allowed range of variation for the free parameters.

The resulting points of this second scan are plotted in Figure 9 in the plane  $\sigma \times BR_{h \rightarrow \gamma\gamma}$  in the gluon fusion production mode (left panel) and the VBF/VH production mode (right panel) vs  $m_h$ , superimposed on the public exclusion limits of CMS collaboration. For convenience only the red points, *i.e.* the points passing all of the indirect, LEP and LHC constraints, are plotted here. The results confirm our expectation from Figures 6 and 7 that there is no sensitivity in the gluon fusion production mode but many points are above the CMS observed limit in the VBF/VH production mode for a light Higgs boson with mass below 105 GeV.

As the points above the observed CMS upper limit are excluded at 95% C.L., we can expect to exclude some new region in the parameter space thanks to this analysis. To illustrate this point, in Figure 10 we plot the points resulting from the previous scan (see Table 8) and passing the three sets of constraints in the plane  $\tan \beta$  vs  $\sin(\beta - \alpha)$  (left panel) and in the plane  $\tan \beta$  vs  $m_h$  (right panel). The violet points have a value of  $\sigma_{VBF/VH} \times BR_{h \rightarrow \gamma\gamma}$  below the CMS observed upper limit for the corresponding mass; the orange points have a value of  $\sigma_{VBF/VH} \times BR_{h \rightarrow \gamma\gamma}$  above the CMS observed upper limit and are consequently excluded by the experiment.

The left panel shows that most of the orange points cluster in an exclusion band in the region  $\tan \beta \in [3;6]$ ,  $\sin(\beta - \alpha) \in [-0.27;-0.14]$ . However, we cannot conclude that the whole orange band is excluded as we have many free parameters: the plot shows in fact a projection of a five-dimensional space on a plane. Therefore, we can have multiple points with a same value of  $\tan \beta$  and  $\sin(\beta - \alpha)$  but with different values for the other free parameters, producing violet and orange points at the same position in this specific plane. Hence the orange band in the left plot of Figure 10 cannot be taken as an absolute exclusion area.

In order to illustrate this point, we produce two additional plots, shown in Figure 11, in the plane  $\tan \beta$  versus  $\sin(\beta - \alpha)$  with all the other free parameters fixed. We choose

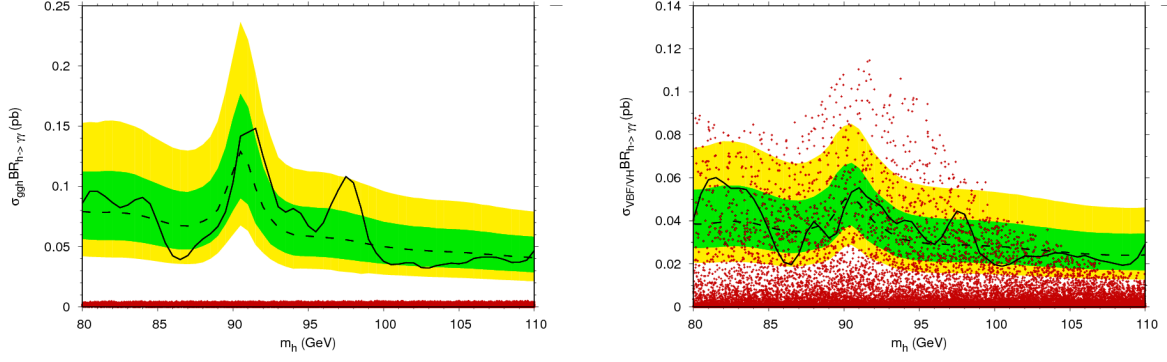


**Figure 9:** Points generated in the 2HDM Type I passing indirect, LEP and LHC constraints, superimposed on the results of the CMS 8 TeV low-mass di-photon analysis [11] in the gluon fusion production mode (left panel) and the combined VBF and VH production mode (right panel). The dashed line corresponds to the expected upper limit on  $\sigma \times BR_{h \rightarrow \gamma\gamma}$  at 95% C.L., with 1 and 2 sigma errors in green and yellow respectively. The solid line is the observed upper limit at 95% C.L.

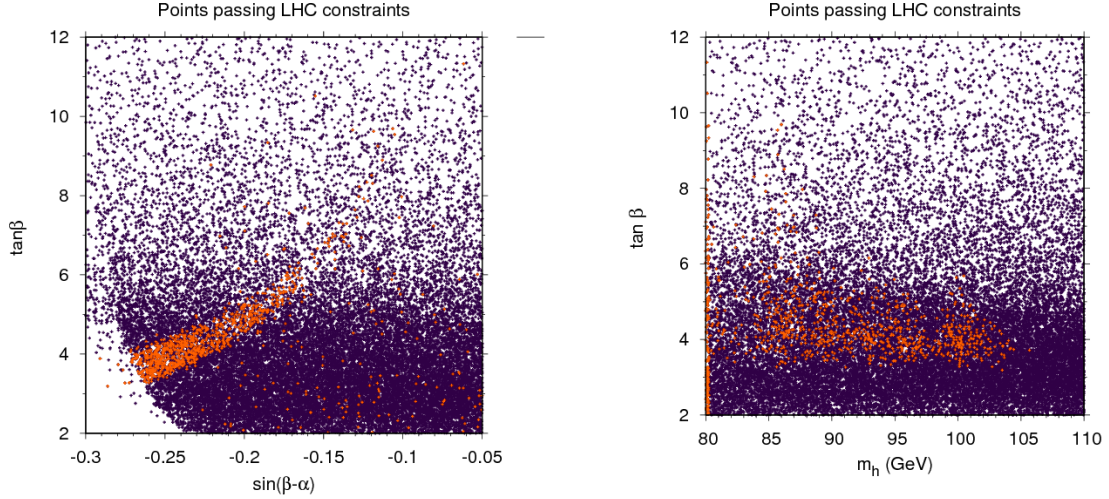


**Figure 10:** Projection of the points resulting from the previous scan (see Table 8) and passing indirect, LEP and LHC constraints in the plane  $\tan \beta$  vs  $\sin(\beta - \alpha)$  (left) and  $\tan \beta$  vs  $m_h$  (right). The points with a value of  $\sigma_{VBF/VH} \times BR_{h \rightarrow \gamma\gamma}$  above the CMS observed 95% C.L. upper limit are in orange; the others are in violet.

$m_h = 87$  GeV,  $m_H = 125$  GeV,  $m_{12} = 30$  GeV and perform this scan for two different values of the mass of the pseudo-scalar and charged Higgs bosons:  $m_A = m_{H^\pm} = 80$  GeV (left panel) and  $m_A = m_{H^\pm} = 500$  GeV (right panel). As before, we only consider points passing the indirect, LEP and LHC constraints. The color code is the same as in Figure 10. The exclusion zone does not have the same shape in the two different scans and we can see that the violet points

in the left panel are in orange in the panel on the right. It means that we are able to exclude some region in the plane  $\tan\beta$  vs  $\sin(\beta - \alpha)$  but the shape and extent of the exclusion zone depends on the value of the other free parameters.

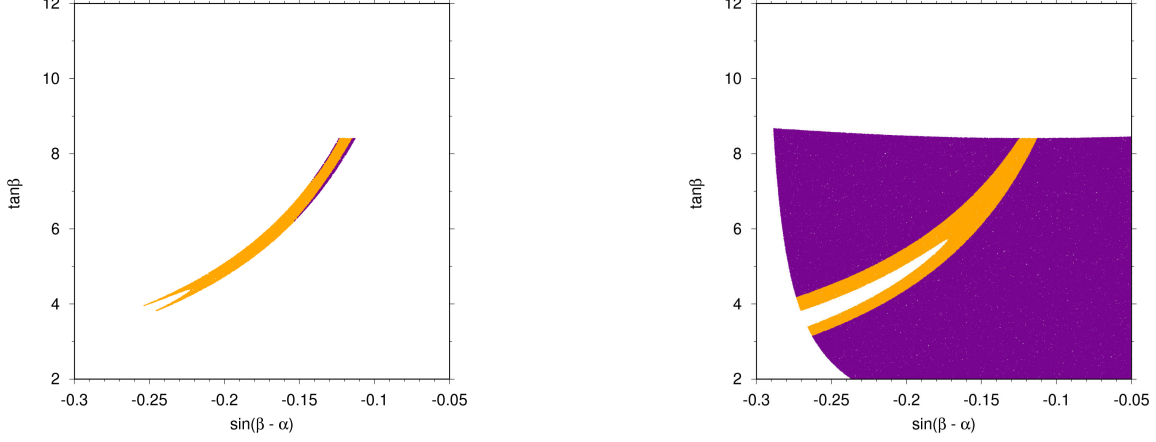


**Figure 11:** Projection of the points passing indirect, LEP and LHC constraints in the plane  $\tan\beta$  vs  $\sin(\beta - \alpha)$  with  $m_h = 87$  GeV,  $m_H=125$  GeV and  $m_{12}=30$  GeV. The mass of the pseudo-scalar and charged Higgs bosons are taken to  $m_A = m_{H^\pm}=80$  GeV (left panel) and  $m_A = m_{H^\pm}=500$  GeV (right panel). Same color code as Figure 10.

Finally, in Figure 12, we show an exclusion zone in the plane  $\tan\beta$  vs  $m_h$  in the particular case where  $m_H = 125$  GeV,  $m_A = m_{H^\pm} = 80$  GeV,  $\sin(\beta - \alpha)=-0.2$  and  $m_{12} = 30$  GeV. The orange points are excluded by the CMS low mass di-photon analysis at 95% C.L..

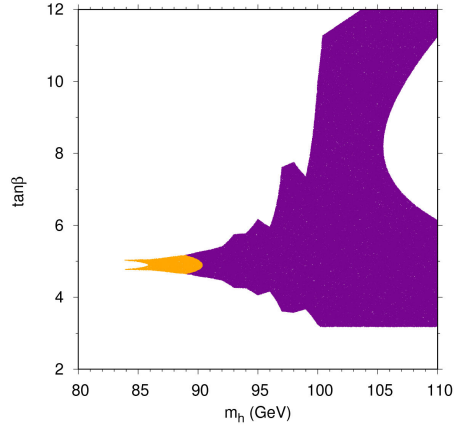


**Figure 12:** Projection of the points passing indirect, LEP and LHC constraints in the plane  $\tan\beta$  vs  $m_h$  with  $m_H=125$  GeV,  $m_A = m_{H^\pm}=80$  GeV,  $\sin(\beta - \alpha)=-0.2$  and  $m_{12}=30$  GeV. Same color code as Figure 10.

## 5 Search for a light pseudo-scalar Higgs boson in the 2HDMs

In the previous section we have seen that values of the pseudo-scalar  $A$  masses below 110 GeV are allowed in Type I and Lepton Specific models. It is thus natural to ask if the di-photon resonant signal may be due to the decays of the pseudo-scalar instead of the light scalar  $h$ . In this section we will pursue this possibility, limiting ourselves to the same configuration studied above, i.e. fixing the mass of the heavy Higgs boson  $H$  to  $m_H = 125$  GeV. The constraints on the free parameters of the model coming from indirect, LEP and LHC constraints obtained in section 4.2 are also valid in the case of a pseudo-scalar. We can therefore focus on the predicted cross sections for the pseudo-scalar.

As the kinematic behaviour of the two photons coming from the decay of a pseudo-scalar particle is very similar to the one coming from a scalar particle [40], we can directly apply the CMS study as for the scalar case to constrain a possible light pseudo-scalar. The pseudo-scalar  $A$  does not couple at tree level to the W and Z bosons, therefore we will only focus on the gluon fusion production mode. Note also that the mass of the other light scalar  $h$  is left free, and in principle it can also contribute to the signal at the same time as the pseudo-scalar. To simplify the analysis, however, we will not consider the possible bounds coming from  $h$  in this case (as the available parameter space we discuss in the following gives very small cross section times branching for the pseudo-scalar  $A$  which can not be probed at present).

### 5.1 Computation of the cross-section value

The production cross section of the pseudo-scalar is different from the one for the scalar case. It is clear that for example the effective vertex with the gluons will be different due to different couplings and to the absence of couplings with the gauge bosons. However the “kappa trick” technique used for a scalar can be used here too:

$$\sigma_{ggA}^{2HDM} \simeq \kappa_g^2 \times \sigma_{ggA}^{SM}, \quad \kappa_g^2 = \frac{\Gamma_{A \rightarrow gg}^{2HDM}}{\Gamma_{A \rightarrow gg}^{SM}} \quad (5.1)$$

where the label  $SM$  indicates that the couplings of the pseudo-scalar are set to be equal to the SM couplings of the Higgs boson (except for the different  $\mathcal{CP}$  properties). However the values of  $\sigma_{ggA}^{SM}$  are not available from the LHC Higgs Cross-Section Working Group and we cannot assume that they are the same as those of the cross section of the SM scalar Higgs boson  $\sigma_{ggh}^{SM}$ . Furthermore the program 2HDMC does not supply the value of  $\Gamma_{A \rightarrow gg}^{SM}$ .

We resolve the first issue by obtaining the values of the production cross-section in the gluon fusion mode for a pseudo-scalar with SM-like couplings from **SusHi** for a discrete set of values and then interpolating between the obtained values to obtain a smooth function. Figure 13 shows the significant difference between the cross section obtained from **SusHi** in the gluon fusion production mode at NNLO for an SM scalar particle (in violet) and for an SM-like pseudo-scalar particle (in green) plotted as a function of the mass of the spin-0 particle.

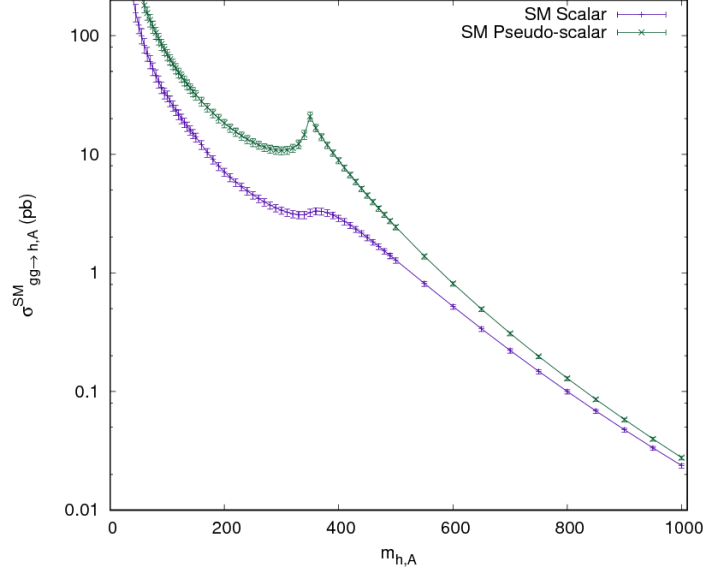


**Figure 13:** Production cross section in gluon fusion mode computed at NNLO by **SusHi** for an SM scalar particle (in violet) and for an SM pseudo-scalar particle (in green).

The second issue can be overcome by using an analytical computation. The pseudo-scalar  $A$  couples to the quarks as  $g_{Aqq} = g_q^A \times i \frac{m_q}{v} \times i \gamma_5$  with  $g_q^A = 1$  in the SM-like case and  $g_q^A = \tan \beta$  or  $\cot \beta$  in the 2HDM case (see Table 2). The decay width of a pseudo-scalar  $A$  into two gluons can therefore be written at LO as [41]:

$$\Gamma_{A \rightarrow gg} = \frac{G_F \alpha_s^2 m_A^3}{16 \sqrt{2} \pi^3} \left| \sum_q g_q^A A_f^A(\tau_q) \right|^2 \quad (5.2)$$

with  $\tau_q \equiv m_A^2 / 4m_q^2$  and  $A_f^A$  the fermionic amplitude defined as:

$$A_f^A(\tau) = \frac{f(\tau)}{\tau}, \quad f(\tau) = \begin{cases} \arcsin^2 \sqrt{\tau} & \tau \leq 1 \\ -\frac{1}{4} \left[ \log \left( \frac{1 + \sqrt{1 - 1/\tau}}{1 - \sqrt{1 - 1/\tau}} \right) - i\pi \right]^2 & \tau > 1 \end{cases} \quad (5.3)$$

The NLO corrections in the heavy top limit can be written as an additional factor to the LO width [41]. Considering only the top and the bottom quarks in the loop, we can then compute the parameter  $\kappa_g^2$  at NLO in Type I:

$$\kappa_g^2 = \frac{\Gamma_{A \rightarrow gg}^{2HDM}}{\Gamma_{A \rightarrow gg}^{SM}} = \frac{\left| \cot \beta \times A_f^A(\tau_t) + \cot \beta \times A_f^A(\tau_b) \right|^2}{\left| A_f^A(\tau_t) + A_f^A(\tau_b) \right|^2} \quad (5.4)$$

Using the values of  $\sigma_{ggA}^{SM}$  from **SusHi** and the analytic value of  $\kappa_g^2$  given above we are now able to compute the value of  $\sigma_{ggA}^{2HDM}$  for any possible value of the free parameters.

In order to check the validity of the method, we compare the cross-section values obtained with the “kappa trick” method with the ones given by **SusHi**. We give the results for  $m_h = 87$  GeV,  $m_H = 125$  GeV,  $m_{H^\pm} = 500$  GeV,  $\tan\beta = 8$ ,  $\sin(\beta - \alpha) = -0.2$  and  $m_{12} = 30$  GeV in Figure 14. In the left panel the mass  $m_A$  ranges from 60 GeV to 1000 GeV, while the right panel is a zoom in the mass region of interest for the study of a light pseudo-scalar. The dashed blue line corresponds to the cross section computed with the “kappa trick”, the dotted red line to the one computed with **SusHi** and the green solid line to the deviation between the two methods. At low mass the deviation is below 10%, which is low enough with respect to the current uncertainties to be used in an analysis. Above  $m_A = 120$  GeV the deviation grows significantly and is about 24% at  $m_A = 1000$  GeV. This is due to the NLO corrections in the “kappa trick” which only consider corrections in the infinite top mass approximation. As  $m_A$  grows, this approximation becomes invalid and the cross-section value diverges from **SusHi**’s results.

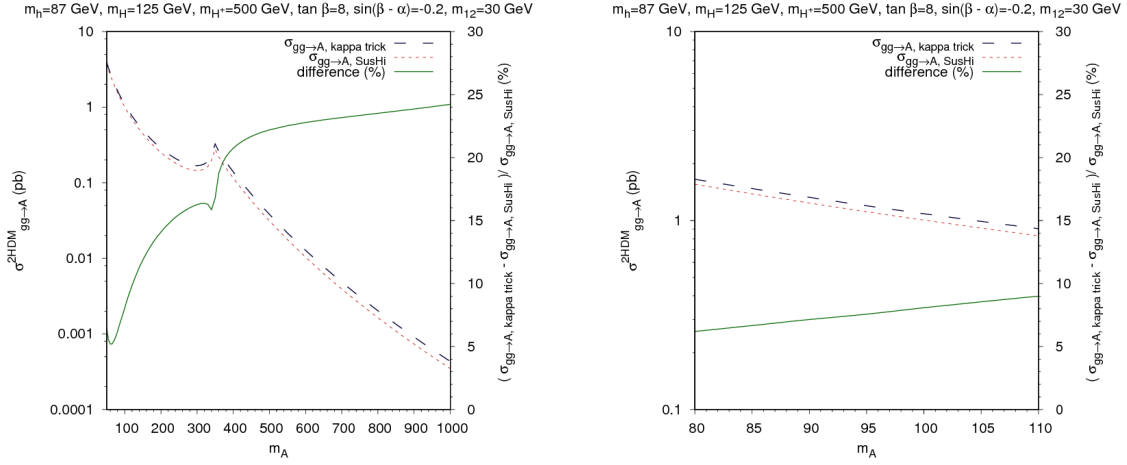


**Figure 14:**  $\sigma_{gg \rightarrow A}^{2HDM}$  computed with the “kappa trick” (dashed blue line) and with **SusHi** (dotted red line). The right panel is a zoom of the left one in the low mass range.

## 5.2 Comparison with the CMS low mass di-photon analysis.

The constraints on the free parameters coming from indirect, LEP and LHC constraints obtained in section 4.2 remain valid for the study of a light pseudo-scalar in the scenario where the heavy scalar is identified with the SM-like one at 125 GeV. We can therefore perform a new scan using these bounds, with the additional constraint that the pseudo-scalar must have a mass between 80 GeV and 110 GeV in order to fit with the available range of the CMS analysis. The range of variation for the free parameters are given in Table 9. We restrict ourselves to Type I only in the gluon fusion production mode.

As for the scalar study we apply the indirect, LEP and LHC constraints. The resulting points are plotted in red in the plane  $\sigma_{gg \rightarrow A} \times BR_{A \rightarrow \gamma\gamma}$  vs  $m_A$  and superimposed on the CMS

results in Figure 15.

$m_h$ (GeV)	$m_H$ (GeV)	$m_A$ (GeV)	$m_{H^\pm}$ (GeV)	$\sin(\beta - \alpha)$	$\tan \beta$	$m_{12}$ (GeV)
[80; 110]	125	[80; 110]	[80; 630]	[-0.4; 0.3]	[1.5; 50]	$[-(300)^2; +(100)^2]$

**Table 9:** Range of variation for the free parameters used in the study of the pseudo-scalar A.

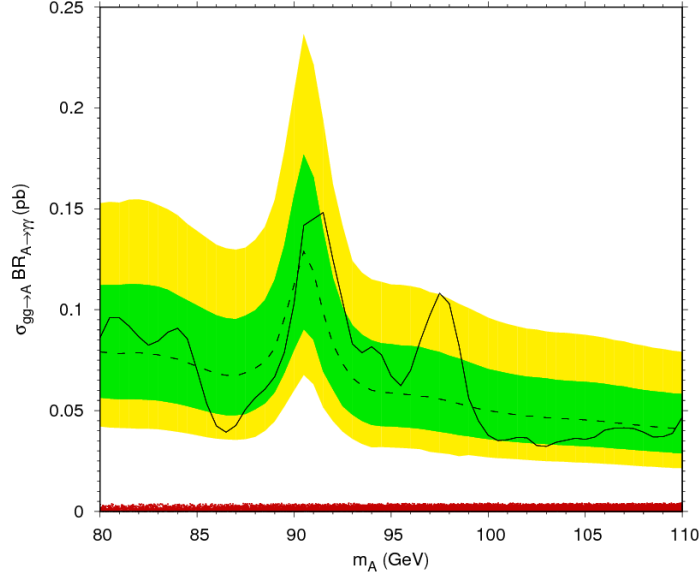


**Figure 15:** Points generated in the 2HDM Type I passing indirect, LEP and LHC constraints, superimposed on the CMS 8 TeV low-mass di-photon analysis [11] in the gluon fusion production mode. The dashed line corresponds to the expected upper limit at 95% C.L.. The solid line is the observed upper limit at 95% C.L..

We can see that the points are well below the CMS observed upper limit on production cross section times branching ratio at 95% C.L.. We therefore conclude that CMS had no sensitivity to a light pseudo-scalar during the LHC Run 1 in the di-photon final state.

## 6 Conclusions

The search for an extended Higgs sector is ongoing at the LHC and represents one of the most important avenues for probing the possible structure of physics beyond the Standard Model. In the simplified setting of Two Higgs Doublet Models, we have explored current constraints from flavour, precision electroweak tests and direct collider searches. We have tested the possible reach of the CMS experiment at the LHC Run 1 for a second Higgs particle lighter than the 125 GeV Higgs boson already discovered. We have explored in detail the different production modes (gluon fusion, vector boson fusion, associated production with a gauge boson) and the subsequent decay to two photons for the light boson. We have found that some sensitivity in these last two production modes is expected even simply recasting an existing Run 1 CMS analysis. A lighter (than the 125 GeV Higgs boson) neutral scalar or pseudo-scalar particle is not completely excluded by present bounds and searches. Out of the four types of 2HDMs, in the low-mass region for a neutral scalar, only Type I has in its parameter space points with large enough cross section times branching ratio to allow detection or exclusion in the  $\gamma\gamma$  decay channel by this analysis. We have applied this analysis also to the case of a light neutral pseudo-scalar, for which however cross section times branching ratio in the  $\gamma\gamma$  channel is below reach at present. It is however interesting to perform such a low mass analysis (even possibly for lower masses than those considered at Run 1) at 13 TeV for the LHC in Run 2 as the increased sensitivity to lower cross section values will allow to further explore and constrain or possibly discover new scalar or pseudo-scalar neutral particles and in any case allow a better understanding of an extended Higgs sector.

## Acknowledgment

We wish to thank Alexandre Arbey for discussions on the flavour bounds used in the present paper. J.T. acknowledges support from the National Natural Science Foundation of China (number 11505208) and the China Ministry of Science and Technology (number 2013CB838700). We also acknowledge partial support from the Labex-LIO (Lyon Institute of Origins) under grant ANR-10-LABX-66, FRAMA (FR3127, Fédération de Recherche “André Marie Ampère”) and the Theory LHC-France project.



## Appendix

We list in this appendix some extra numerical results in the form of plots used for the validation of the analysis.

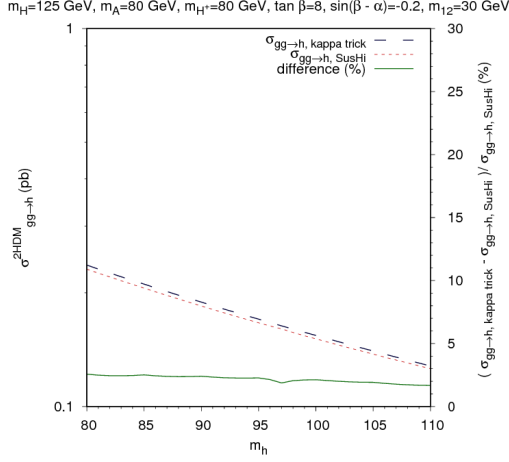


**Figure 16:**  $\sigma^{2HDM}_{gg \rightarrow h}$  for the light Higgs boson as a function of  $m_h$  computed with the “kappa trick” (dashed blue line) and with SusHi (dotted red line) and the deviation between the two (solid green line).

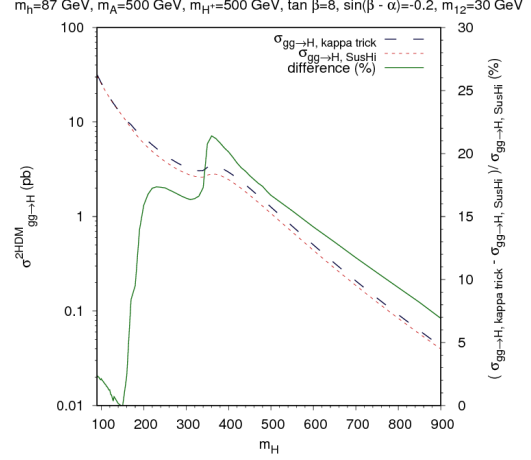


**Figure 17:**  $\sigma^{2HDM}_{gg \rightarrow H}$  for the heavy Higgs boson as a function of  $m_H$  computed with the “kappa trick” (dashed blue line) and with SusHi (dotted red line) and the deviation between the two (solid green line). As the approximation of the infinite mass for the top quark becomes false, the results with “kappa trick” move away from SusHi’s results.

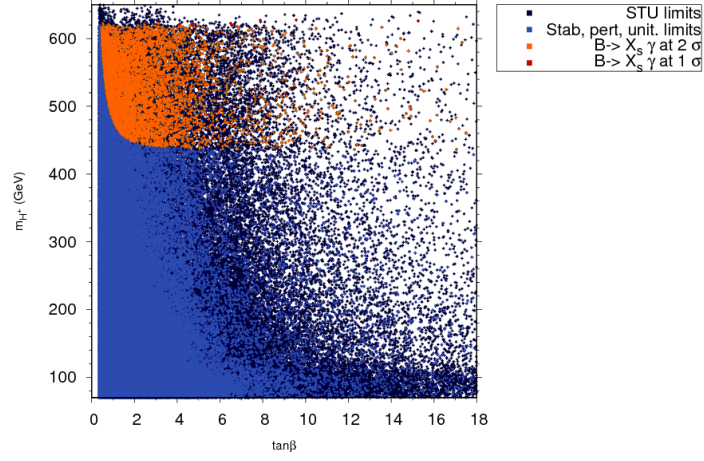


**Figure 18:** Points passing the S, T, U limits (dark blue), stability, perturbativity and unitarity limits (light blue) and  $\mathcal{BR}(B \rightarrow X_s \gamma)$  flavor constraints at  $1\sigma$  (red) and  $2\sigma$  (yellow). The constraint on  $\mathcal{BR}(B \rightarrow X_s \gamma)$  imposes a very hard bound on the mass of the charged Higgs bosons.

## References

- [1] **ATLAS** Collaboration, G. Aad *et al.*, “Observation of a new particle in the search for the Standard Model Higgs boson with the ATLAS detector at the LHC,” [\*Phys. Lett.\* \*\*B716\*\* \(2012\) 1–29](#), [arXiv:1207.7214 \[hep-ex\]](#).
- [2] **CMS** Collaboration, S. Chatrchyan *et al.*, “Observation of a new boson at a mass of 125 GeV with the CMS experiment at the LHC,” [\*Phys. Lett.\* \*\*B716\*\* \(2012\) 30–61](#), [arXiv:1207.7235 \[hep-ex\]](#).
- [3] P. M. Ferreira, R. Santos, M. Sher, and J. P. Silva, “Could the LHC two-photon signal correspond to the heavier scalar in two-Higgs-doublet models?,” [\*Phys. Rev.\* \*\*D85\*\* \(2012\) 035020](#), [arXiv:1201.0019 \[hep-ph\]](#).
- [4] S. Chang, S. K. Kang, J.-P. Lee, K. Y. Lee, S. C. Park, and J. Song, “Comprehensive study of two Higgs doublet model in light of the new boson with mass around 125 GeV,” [\*JHEP\* \*\*05\*\* \(2013\) 075](#), [arXiv:1210.3439 \[hep-ph\]](#).
- [5] S. Chang, S. K. Kang, J.-P. Lee, K. Y. Lee, S. C. Park, and J. Song, “Two Higgs doublet models for the LHC Higgs boson data at  $\sqrt{s} = 7$  and 8 TeV,” [\*JHEP\* \*\*09\*\* \(2014\) 101](#), [arXiv:1310.3374 \[hep-ph\]](#).
- [6] A. Celis, V. Ilisie, and A. Pich, “LHC constraints on two-Higgs doublet models,” [\*JHEP\* \*\*07\*\* \(2013\) 053](#), [arXiv:1302.4022 \[hep-ph\]](#).
- [7] G. Cacciapaglia, A. Deandrea, G. Drieu La Rochelle, and J.-B. Flament, “Searching for a lighter Higgs boson: Parametrization and sample tests,” [\*Phys. Rev.\* \*\*D91\*\* no. 1, \(2015\) 015012](#), [arXiv:1311.5132 \[hep-ph\]](#).
- [8] J. Bernon, J. F. Gunion, H. E. Haber, Y. Jiang, and S. Kraml, “Scrutinizing the alignment limit in two-Higgs-doublet models. II.  $m_H=125\text{GeV}$ ,” [\*Phys. Rev.\* \*\*D93\*\* no. 3, \(2016\) 035027](#), [arXiv:1511.03682 \[hep-ph\]](#).
- [9] J. Bernon, J. F. Gunion, Y. Jiang, and S. Kraml, “Light Higgs bosons in Two-Higgs-Doublet Models,” [\*Phys. Rev.\* \*\*D91\*\* no. 7, \(2015\) 075019](#), [arXiv:1412.3385 \[hep-ph\]](#).
- [10] U. Ellwanger and M. Rodriguez-Vazquez, “Discovery Prospects of a Light Scalar in the NMSSM,” [\*JHEP\* \*\*02\*\* \(2016\) 096](#), [arXiv:1512.04281 \[hep-ph\]](#).
- [11] **CMS** Collaboration, “Search for new resonances in the diphoton final state in the mass range between 80 and 110 GeV in pp collisions at  $\sqrt{s} = 8$  TeV,” Tech. Rep. CMS-PAS-HIG-14-037, CERN, Geneva, 2015. <http://cds.cern.ch/record/2063739>.
- [12] **ATLAS** Collaboration, G. Aad *et al.*, “Search for Scalar Diphoton Resonances in the Mass Range 65 – 600 GeV with the ATLAS Detector in  $pp$  Collision Data at  $\sqrt{s} = 8$  TeV,” [\*Phys. Rev. Lett.\* \*\*113\*\* no. 17, \(2014\) 171801](#), [arXiv:1407.6583 \[hep-ex\]](#).
- [13] G. C. Branco, P. M. Ferreira, L. Lavoura, M. N. Rebelo, M. Sher, and J. P. Silva, “Theory and phenomenology of two-Higgs-doublet models,” [\*Phys. Rept.\* \*\*516\*\* \(2012\) 1–102](#), [arXiv:1106.0034 \[hep-ph\]](#).
- [14] M. E. Peskin and T. Takeuchi, “Estimation of oblique electroweak corrections,” [\*Phys. Rev.\* \*\*D46\*\* \(1992\) 381–409](#).

- [15] D. Eriksson, J. Rathsmann, and O. Stal, “2HDMC: Two-Higgs-Doublet Model Calculator Physics and Manual,” [\*Comput. Phys. Commun.\* \*\*181\*\* \(2010\) 189–205](#), [arXiv:0902.0851 \[hep-ph\]](#).
- [16] **Gfitter Group** Collaboration, M. Baak, J. Cth, J. Haller, A. Hoecker, R. Kogler, K. Mnig, M. Schott, and J. Stelzer, “The global electroweak fit at NNLO and prospects for the LHC and ILC,” [\*Eur. Phys. J. C\* \*\*74\*\* \(2014\) 3046](#), [arXiv:1407.3792 \[hep-ph\]](#).
- [17] A. Arhrib, R. Benbrik, and N. Gaur, “ $H \rightarrow \gamma\gamma$  in Inert Higgs Doublet Model,” [\*Phys. Rev.\* \*\*D85\*\* \(2012\) 095021](#), [arXiv:1201.2644 \[hep-ph\]](#).
- [18] F. Mahmoudi, “SuperIso v2.3: A Program for calculating flavor physics observables in Supersymmetry,” [\*Comput. Phys. Commun.\* \*\*180\*\* \(2009\) 1579–1613](#), [arXiv:0808.3144 \[hep-ph\]](#).
- [19] F. Mahmoudi, “SuperIso: A Program for calculating the isospin asymmetry of  $B \rightarrow \ell K^* \gamma$  in the MSSM,” [\*Comput. Phys. Commun.\* \*\*178\*\* \(2008\) 745–754](#), [arXiv:0710.2067 \[hep-ph\]](#).
- [20] **Heavy Flavor Averaging Group (HFAG)** Collaboration, Y. Amhis et al., “Averages of  $b$ -hadron,  $c$ -hadron, and  $\tau$ -lepton properties as of summer 2014,” [arXiv:1412.7515 \[hep-ex\]](#).
- [21] T. Hurth, F. Mahmoudi, and S. Neshatpour, “On the anomalies in the latest LHCb data,” [\*Nucl. Phys.\* \*\*B909\*\* \(2016\) 737–777](#), [arXiv:1603.00865 \[hep-ph\]](#).
- [22] **LHCb** Collaboration, R. Aaij et al., “Measurement of the  $B_s^0 \rightarrow \mu^+ \mu^-$  branching fraction and search for  $B^0 \rightarrow \mu^+ \mu^-$  decays at the LHCb experiment,” [\*Phys. Rev. Lett.\* \*\*111\*\* \(2013\) 101805](#), [arXiv:1307.5024 \[hep-ex\]](#).
- [23] **LHCb**, **CMS** Collaboration, V. Khachatryan et al., “Observation of the rare  $B_s^0 \rightarrow \mu^+ \mu^-$  decay from the combined analysis of CMS and LHCb data,” [\*Nature\* \*\*522\*\* \(2015\) 68–72](#), [arXiv:1411.4413 \[hep-ex\]](#).
- [24] **Particle Data Group** Collaboration, K. A. Olive et al., “Review of Particle Physics,” [\*Chin. Phys.\* \*\*C38\*\* \(2014\) 090001](#).
- [25] A. Lenz, “ $B$ -mixing in and beyond the Standard model,” in [8th International Workshop on the CKM Unitarity Triangle \(CKM2014\) Vienna, Austria, September 8-12, 2014](#), 2014. [arXiv:1409.6963 \[hep-ph\]](#).  
<https://inspirehep.net/record/1318833/files/arXiv:1409.6963.pdf>.
- [26] P. Bechtle, O. Brein, S. Heinemeyer, G. Weiglein, and K. E. Williams, “HiggsBounds: Confronting Arbitrary Higgs Sectors with Exclusion Bounds from LEP and the Tevatron,” [\*Comput. Phys. Commun.\* \*\*181\*\* \(2010\) 138–167](#), [arXiv:0811.4169 \[hep-ph\]](#).
- [27] P. Bechtle, O. Brein, S. Heinemeyer, G. Weiglein, and K. E. Williams, “HiggsBounds 2.0.0: Confronting Neutral and Charged Higgs Sector Predictions with Exclusion Bounds from LEP and the Tevatron,” [\*Comput. Phys. Commun.\* \*\*182\*\* \(2011\) 2605–2631](#), [arXiv:1102.1898 \[hep-ph\]](#).
- [28] P. Bechtle et al., “Recent Developments in HiggsBounds and a Preview of HiggsSignals,” [\*PoS CHARGED2012\* \(2012\) 024](#), [arXiv:1301.2345 \[hep-ph\]](#).
- [29] P. Bechtle et al., “HiggsBounds-4: Improved Tests of Extended Higgs Sectors against Exclusion Bounds from LEP, the Tevatron and the LHC,” [\*Eur. Phys. J. C\* \*\*74\*\* \(2014\) 2693](#), [arXiv:1311.0055 \[hep-ph\]](#).

- [30] **ATLAS, CMS** Collaboration, G. Aad *et al.*, “Measurements of the Higgs boson production and decay rates and constraints on its couplings from a combined ATLAS and CMS analysis of the LHC  $pp$  collision data at  $\sqrt{s} = 7$  and 8 TeV,” [arXiv:1606.02266 \[hep-ex\]](#).
- [31] J.-B. Flament, “Higgs Couplings and BSM Physics: Run I Legacy Constraints,” [arXiv:1504.07919 \[hep-ph\]](#).
- [32] R. V. Harlander, S. Liebler, and H. Mantler, “SusHi Bento: Beyond NNLO and the heavy-top limit,” [arXiv:1605.03190 \[hep-ph\]](#).
- [33] **LHC Higgs Cross Section Working Group** Collaboration, J. R. Andersen *et al.*, “Handbook of LHC Higgs Cross Sections: 3. Higgs Properties,” [arXiv:1307.1347 \[hep-ph\]](#).
- [34] G. Cacciapaglia, A. Deandrea, and J. Llodra-Perez, “Higgs to Gamma Gamma beyond the Standard Model,” [JHEP](#) **06** (2009) 054, [arXiv:0901.0927 \[hep-ph\]](#).
- [35] G. Cacciapaglia, A. Deandrea, G. Drieu La Rochelle, and J.-B. Flament, “Higgs couplings: disentangling New Physics with off-shell measurements,” [Phys. Rev. Lett.](#) **113** no. 20, (2014) 201802, [arXiv:1406.1757 \[hep-ph\]](#).
- [36] A. Buckley, J. Ferrando, S. Lloyd, K. Nordström, B. Page, M. Rfenacht, M. Schnherr, and G. Watt, “LHAPDF6: parton density access in the LHC precision era,” [Eur. Phys. J.](#) **C75** (2015) 132, [arXiv:1412.7420 \[hep-ph\]](#).
- [37] J. Butterworth *et al.*, “PDF4LHC recommendations for LHC Run II,” [J. Phys.](#) **G43** (2016) 023001, [arXiv:1510.03865 \[hep-ph\]](#).
- [38] R. Harlander, M. Mhlleitner, J. Rathsmann, M. Spira, and O. Stl, “Interim recommendations for the evaluation of Higgs production cross sections and branching ratios at the LHC in the Two-Higgs-Doublet Model,” [arXiv:1312.5571 \[hep-ph\]](#).
- [39] **LEP, DELPHI, OPAL, ALEPH, L3** Collaboration, G. Abbiendi *et al.*, “Search for Charged Higgs bosons: Combined Results Using LEP Data,” [Eur. Phys. J.](#) **C73** (2013) 2463, [arXiv:1301.6065 \[hep-ex\]](#).
- [40] P. Artoisenet *et al.*, “A framework for Higgs characterisation,” [JHEP](#) **11** (2013) 043, [arXiv:1306.6464 \[hep-ph\]](#).
- [41] M. Spira, A. Djouadi, D. Graudenz, and P. M. Zerwas, “Higgs boson production at the LHC,” [Nucl. Phys.](#) **B453** (1995) 17–82, [arXiv:hep-ph/9504378 \[hep-ph\]](#).